

Curvature as a guiding field for patterns in thin block copolymer films

Giang Thi Vu,^{1,*} Anabella A. Abate,² Leopoldo R. Gómez,² Aldo D. Pezzutti,² Richard A. Register,³ Daniel A. Vega,^{2,†} and Friederike Schmid^{1,‡}

¹*Institut für Physik, Johannes Gutenberg Universität Mainz Staudinger Weg 7, D-55099 Mainz, Germany*

²*Department of Physics, Universidad Nacional del Sur - IFISUR CONICET, 800, Bahía Blanca, Argentina*

³*Department of Chemical and Biological Engineering, Princeton University, Princeton, New Jersey, 08544, USA*

Experimental data on thin films of cylinder-forming block copolymers (BC) – free-standing BC membranes as well as supported BC films – strongly suggest that the local orientation of the BC patterns is coupled to the geometry in which the patterns are embedded. We analyze this phenomenon using general symmetry considerations and numerical self-consistent field studies of curved BC films in cylindrical geometry. The stability of the films against curvature-induced dewetting is also analyzed. In good agreement with experiments, we find that the BC cylinders tend to align along the direction of curvature at high curvatures. At low curvatures, we identify a transition from perpendicular to parallel alignment in supported films, which is absent in free-standing membranes. Hence both experiments and theory show that curvature can be used to manipulate and align BC patterns.

Because of their ability to self-assemble into well-defined periodic nanostructures, block copolymers (BC) are attracting great interest as potential template materials for cost-effective nanofabrication techniques [1–9]. With BC systems, one can produce high-resolution patterns with tunable wavelength using traditional processing techniques. This offers promising perspectives for applications in scalable nanoscale devices. However, one frequent problem with the self-assembly approach is lack of long-range order due to pattern undulations and defects, e.g., dislocations, disclinations, or grain boundaries [1, 10–13]. Numerous methods to produce patterns with well-defined orientational and positional order have been proposed, such as shear alignment [14–16], alignment in electric fields [17–19], zone annealing [20, 21], or grapho- and chemo-epitaxy, where surface interactions and confinement effects are exploited to order patterns [6–8, 14, 21–27] or to control defect positions [28].

Here, we analyze another possible source of alignment, the *geometry* in which the system is embedded. Experiments and simulations on curved systems have indicated that the pattern configurations are affected by both intrinsic and extrinsic geometry. Even in Euclidean systems, a strong coupling between patterns and curvature seems to drive the equilibrium configurations and the coarsening process [7, 23, 29, 30].

As a first step towards a more quantitative understanding of the nature of the coupling between BC thin films or membranes and curvature, in the present paper, we study curved monolayers of cylinder-forming BC systems by complementary experiments, symmetry considerations, and self-consistent field theory (SCFT) calculations [9, 31]. We consider two types of model systems: a) free-standing BC membranes and b) BC thin films deposited onto a curved substrate.

The geometric features of a 2D curved surface can be characterized in terms of a shape operator \mathbf{S} , which has two Eigenvalues $k_{1,2} = 1/R_{1,2}$ corresponding to the in-

verse maximal and minimal radii of curvature R_i [see Supplemental Material (SM) for more details]. The determinant and the trace of \mathbf{S} define the Gaussian curvature $K = k_1 k_2$ and twice the mean curvature $2H = k_1 + k_2$, respectively [32]. The experimental systems studied here have a non-Euclidean metric ($K \neq 0$, free-standing membrane) or a Euclidean metric with zero Gaussian curvature ($K = 0$, curved substrate).

In both systems we employ the same BC system, a cylinder-forming polystyrene-block-poly(ethylene-alt-propylene) diblock (PS-PEP 4/13) [33]. The number-average block molecular weights for the BC are 4.3 kg/mol for PS and 13.2 kg/mol for PEP. In bulk, the PS blocks arrange in hexagonally packed cylinders embedded in the PEP matrix. In thin films the PS cylinders adopt a configuration parallel to the film surface. The center-to-center spacing of the cylinders is $d_{sm} = 21$ nm. Thin films of thickness ~ 30 nm are prepared by spin-coating from a 1 wt. % solution in toluene, a good solvent for both blocks. Order is induced by annealing at a temperature T , above the glass transition of the PS block ($T_g \sim 330$ K) and below the order-disorder transition temperature $T_{ODT} = 417$ K of the BC. Details of the preparation of the experimental systems are given in SM. To obtain free-standing membranes, the films are first annealed on a flat substrate, then further cooled down below the T_g of the PS block and finally lifted off and re-deposited on a transmission electron microscopy (TEM) grid. During this process, the system retains the symmetry, average inter-cylinder distance, and structure of defects established during annealing. To obtain supported films, the BCs are directly spin-coated onto curved substrates and the thermal annealing process is monitored by atomic force microscopy (AFM) at selected time points.

Fig. 1 shows an AFM image of a free-standing film where height and cylinder locations are measured simultaneously. The light and dark regions correspond to PS-rich and PEP-rich regions, respectively. After releasing

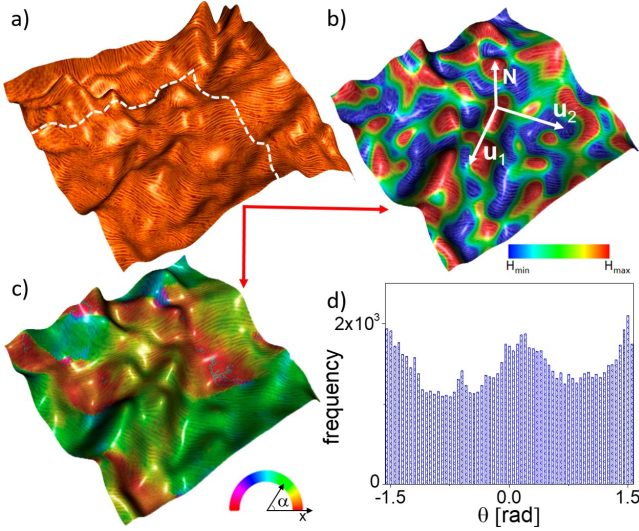


FIG. 1. a) Phase-height AFM image of a free-standing thin film (image size: $2.6 \mu\text{m} \times 2.6 \mu\text{m}$). b) Local mean curvature for the membrane shape. Here the vectors $u_{1,2}$ indicate the directions of the principal curvatures and \mathbf{N} is the normal vector to the membrane surface (image size: $1.8 \mu\text{m} \times 1.8 \mu\text{m}$, region indicated by dashed lines in panel a; $H_{\text{max}} = -H_{\text{min}} = 3.84 \times 10^{-3} \text{ nm}^{-1}$). c) Local orientation of the director field α of the pattern with regard to the x-axis. d) Histogram showing the local distribution of angles $\theta = \alpha - \beta$ between α and the local orientation of the membrane wrinkles β [see also Fig. S2 in SM].

the membrane from the confining substrate, it develops a non-Euclidean shape to relieve the elastic energy of topological defects that have survived the thermal annealing. The shape results from a competition between the strain field of the defects, the bending energy associated with the curvature of the membrane, and the membrane tension [29]. Fig. 1 (d) shows the correlation between the orientation of the underlying pattern and the local orientation of membrane wrinkles. Although the different defects impose competing out-of-plane deformations, one clearly notices that wrinkles have a tendency to be oriented either perpendicular ($\theta = 0$) or parallel ($\theta = \pm\pi/2$) to the underlying cylinders, suggesting that the bending energy is anisotropic and coupled to the liquid crystalline order of the BC [see also Figs. S3, S4 in SM].

A similar observation is made for the thin films on curved substrates. Fig. 2 shows AFM phase and height-phase images of the BC thin film deposited onto a curved substrate. Right after the spin coating, the pattern is characterized by a very small orientational correlation length ($\xi_2 \sim 20 \text{ nm}$) and a high density of defects. During annealing at $T=373 \text{ K}$, the system orders via annihilation of dislocations and disclinations. Already at an early stage of annealing, the thin film becomes unstable and dewets at the regions with the highest curvature (Fig. 2). Upon further annealing, the order in the system increases and the pattern develops a clear preferential

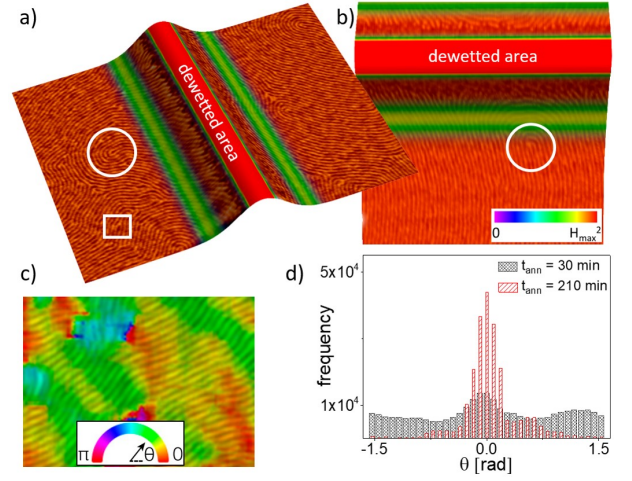


FIG. 2. Top panels: 3D AFM phase-height images of the BC thin film on a curved substrate after annealing at $T=373 \text{ K}$. Panels a) and b) show the pattern configuration after 90 min (image size: $2.0 \mu\text{m} \times 1.5 \mu\text{m}$) and 3.5 h of thermal annealing (image size: $1.0 \mu\text{m} \times 1.25 \mu\text{m}$), respectively. Height scale: 80 nm from crest to valley, $H_{\text{max}}^2 = 6.25 \mu\text{m}^{-2}$. The presence of a dislocation and $+1/2$ disclinations has been emphasized with a rectangle and circles, respectively. Bottom panels: c) Local orientation of the smectic pattern (color map indicated at the bottom). d) Histograms showing the distribution of angles θ between the local cylinder orientation and the direction of curvature at two different annealing times.

orientation with regard to the substrate. Fig. 2 shows that the PS cylinders tend to align perpendicular to the crest of the substrate. Thus the topography of the substrate seems to act as an external field that breaks the azimuthal symmetry [see also Fig. S5 in SM]. Note that the equilibrium configuration obtained here is opposite to that predicted in previous theories for curved columnar phases [34, 35], where it was assumed that bending along the cylinder direction is energetically more costly than bending in the perpendicular direction [35].

The phenomena described above can be analyzed using general symmetry considerations. The curvature free energy per area of *isotropic* fluid-like membranes can be expanded in the invariants of the shape operator \mathbf{S} as $F_{\text{HC}} = \frac{\kappa_b}{2}(2H - c_0)^2 + \kappa_g K$, where κ_b and κ_g are the bending and Gaussian rigidity, respectively, and c_0 is the spontaneous curvature [36, 37]. Here we consider anisotropic *nematic* membranes with in-plane order characterized by a director \mathbf{n} (the orientation of the cylinders), thus additional terms become possible. Including all terms up to second order in \mathbf{S} that are compatible with the in-plane nematic symmetry, i.e., $(\mathbf{n} \cdot \mathbf{S} \cdot \mathbf{n})$, $(\mathbf{n} \cdot \mathbf{S} \cdot \mathbf{n})^2$ [38, 39], and $(\mathbf{S} \cdot \mathbf{n})^2$ [40, 41], we can derive the following expression for the anisotropic part of the curvature free

energy per area [see SM]:

$$F_{\text{ani}} = -\frac{\kappa'}{2}(k_1 - k_2)(2H - c'_0) \cos(2\theta) - \frac{\kappa''}{2}(H^2 - K) \cos(4\theta). \quad (1)$$

Here $\theta \in [0 : \pi/2]$ denotes the angle between the director and the direction of largest curvature k_1 ($|k_1| > |k_2|$), and κ', κ'', c'_0 are anisotropic elastic parameters. In symmetric membranes, c'_0 vanishes ($c'_0 = 0$). We emphasize that Eq. (1) gives the generic form of the free energy of curved nematic films up to second order in the curvatures, which should be generally valid regardless of molecular details. For $\kappa'' > 0$, the second term describes a quadrupolar coupling between the curvature tensor and the director that favors *two* directions of preferential alignment of the director \mathbf{n} along the two principal directions of curvature. Such a competition between two stable/metastable aligned states was also predicted in other continuum models for nematic shells [42, 43]. The first term selects between the two directions.

The results of the symmetry analysis are compatible with the experiments: As discussed above, in the BC membranes, wrinkles form preferentially parallel or perpendicular to the director [Fig. 1 (d)]. Similarly, in the thin films, the distribution of local cylinder orientations θ is bimodal at early annealing time (30 min), with two characteristic peaks separated by $\sim \pi/2$ [Fig. 2(d)]. During the first stage of coarsening, the parallel and perpendicular configurations compete. After long annealing times, C_\perp dominates, and the histogram becomes sharply peaked at the orientation $\theta = 0$, suggesting $\kappa' > 0$ in Eq. (1). We note, however, that supported films are asymmetric and hence the spontaneous curvature parameter c'_0 will very likely not vanish, in which case Eq. (1) predicts that the preferred orientation switches from $\theta = 0$ to $\theta = \pi/2$ in a region of very small curvatures $k_1 \in [0 : c'_0]$. We will discuss this further below.

In order to obtain a more quantitative theoretical description, we use SCFT [31, 44] to study the two systems considered in the experiment, the free-standing membrane and the curved supported thin film. We consider a melt of asymmetric AB diblock copolymer molecules with degree of polymerization N and statistical segment length b at temperature T confined to a curved film of thickness ϵ by two coaxial cylindrical surfaces (see schematics in Fig. 3(a), 4(a), and 4(b)). Periodic or tilted periodic boundary conditions [see SM] are applied in the two in-plane directions.

In the following, lengths and energies are given in units of $R_g^2 = \frac{1}{6}Nb^2$ and Gk_BT , respectively, where k_B is the Boltzmann constant and $G = \rho_c R_g^3$ is the rescaled dimensionless copolymer density in the bulk. The incompatibility between the blocks is specified by the product χN , where χ is the Flory-Huggins parameter. Here we use $\chi N = 20$ and $f = 0.7$ to match the experimental values (f is the volume fraction of the A -block).

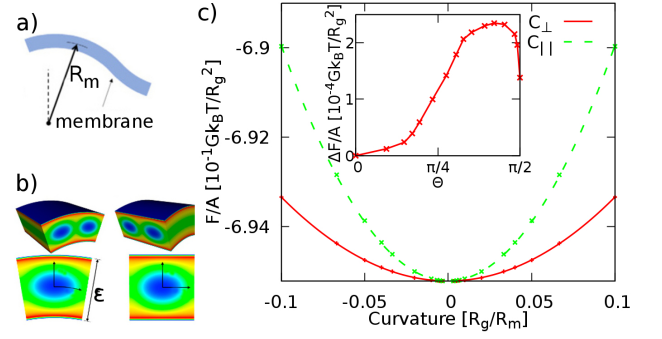


FIG. 3. (a) Schematic representation of curvature radius R_m in free-standing membranes. (b) Density profiles from SCFT for the parallel (left) and perpendicular (right) configurations C_\parallel and C_\perp at $R_m = 9R_g$. (c) Free energy per area as a function of inverse curvature radius R_g/R_m for the C_\parallel and C_\perp configurations. Inset shows the free energy shift per area as a function of angle θ between the cylinders and the direction of curvature relative to the C_\perp configuration ($\theta = 0$) at $R_m = 50R_g$.

Our calculations are done in the grand canonical ensemble with the chemical potential $\mu = (2.55 + \ln G)k_BT$ [9, 45] and inverse isothermal compressibility $\kappa N = 25$ [46, 52, 53]. Monomers $\alpha = A, B$ close to a surface experience a surface field, which we characterize in terms of the surface energy per area γ_α of a fluid of α -monomers in contact with the same surface [see SM], given in units $\hat{\gamma} = Gk_BT/R_g^2$. To account for the experimental fact that cylinders align parallel to the film, the interaction parameters are chosen such that majority A-blocks preferentially adsorb to the surface, i.e., $\gamma_A < \gamma_B$. In planar films, the copolymers then self-assemble into aligned cylinders with a spacing $\lambda = 3.6R_g$. Matching this with the value $d_{sm} = 21$ nm observed experimentally, we can identify $R_g \approx 5.8$ nm [47] and hence $G = 5.77$ for our experimental systems (assuming an average copolymer density of 0.861 g/cm³ at 363K).

We first consider free-standing membranes, which we model as a symmetric film with surface interaction energies $\gamma_A N = -24\hat{\gamma}$ and $\gamma_B N = -23\hat{\gamma}$. We calculate the free energy per area as a function of the curvature radius $1/R_m$ of the mid-surface of the film (see Fig. 3(a) for the two cases where cylinders are aligned parallel or perpendicular to the curvature (C_\parallel, C_\perp , see Fig. 3(b)). In each case, the film thickness ϵ and the wavelength of the characteristic pattern are optimized to obtain the lowest free energy state. Fig. 3(b) shows the resulting density profiles for the parallel and perpendicular configurations in a system with a relatively large curvature ($R_m = 9R_g$). The differences are small, indicating that curvature affects neither the position of the cylinder with regard to the plane of symmetry, nor the segregation strength. The optimum inter-cylinder spacing is $\lambda \sim 3.6R_g$, which is slightly smaller than the bulk value, $\lambda_{bulk} \sim 3.7R_g$. The

ratio, $\lambda/\lambda_{bulk} \sim 0.97$, is in good agreement with SCFT calculations and experiments on flat substrates, where it was found that in thin films the unit cell is stretched perpendicular to the plane of the film resulting in lateral distances smaller than those in bulk [9, 48]. The optimal thickness is $\epsilon \sim 3.5R_g$ for both the parallel and perpendicular configurations [see Fig. S9 in SM]. None of these features appears to be severely affected by the curvature within the range of curvatures explored here.

The behavior of the free energy per area for the two configurations is shown in Fig. 3(c). The perpendicular orientation is clearly favored. Furthermore, in agreement with Eq. (1), both C_\perp and C_\parallel represent local free energy minima with respect to variations of the angle θ between cylinders and the direction of curvature, (see inset of Fig. 3c). Since the free energy grows almost quadratically with the curvature, $F/A = \kappa/2R_m^2$, we can calculate bending stiffness parameters for the C_\parallel and C_\perp configurations. By fitting the free energy per area up to a quadratic order of the mean curvature, we obtain $\kappa_\parallel = (1.056 \pm 0.002)Gk_BT$ and $\kappa_\perp = (0.376 \pm 0.002)Gk_BT$ for the parallel and perpendicular configurations, respectively. Comparing this with Eq. (1) and using $k_1 = \pm 1/R_m$, $k_2 = 0$, we can deduce $\kappa' = (\kappa_\parallel - \kappa_\perp) = 0.68Gk_BT \approx 4k_BT$, which corresponds to $\kappa' \approx 1.6 \times 10^{-13}$ erg at room temperature. In contrast, the total bending energy of the membranes has been estimated to be of order $\kappa_b \sim 10^{-9}$ erg, which is much higher due to the large contribution of the glassy PS block [29]. Hence, the influence of κ' on the membrane shapes is presumably negligible.

The situation is different when looking at copolymer ordering in supported films, where the curvatures are kept fixed and energy differences of order k_BT do significantly influence the selection of the pattern orientations.

Thin films differ from membranes in two respects. First, the reference surface which is kept fixed during the free energy minimization is the interface between the substrate and the film (not the mid-plane of the film as in membranes), and second, the interaction energies may be different at the substrate and air interfaces. Fig. 4(c), 4(d) shows results for $\gamma_B^{a,s} = -6\hat{\gamma}$ and two representative parameter sets for $\gamma_A^{a,s}$: (I) $\gamma_A^s N = -10\hat{\gamma}$, $\gamma_A^a N = -20\hat{\gamma}$, and (II) $\gamma_A^s N = -24\hat{\gamma}$, $\gamma_A^a N = -10\hat{\gamma}$, where superscripts s and a denote “substrate” and “air”, respectively. In both cases, the perpendicular configuration is more favorable at large curvatures. At small curvatures, however, there exists a small regime where parallel configurations have lower free energy. This is in agreement with our symmetry considerations (see above, Eq. (1)) and also with the experimental observations. Indeed, Fig. 2(b) and Fig. S3 in SM suggest that the locally preferred orientation switches from perpendicular to parallel in a region around the inflection point of the surface profile (green shaded areas in Fig. 2), and this induces defects in that region. Hence curvature can be used not only to orient patterns,

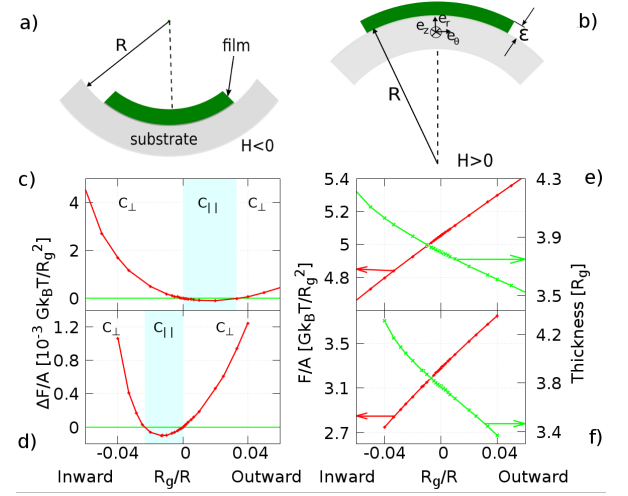


FIG. 4. (a,b) Schematic representation of supported thin films (green) on curved substrates (gray). (c,d) Free energy difference per area $\Delta F = (F_\parallel - F_\perp)/A$ of supported thin films with parallel (C_\parallel) vs. perpendicular (C_\perp) orientation, versus curvature, for two sets of surface interaction energies I (top) and II (bottom) as described in the main text. Blue shaded regions highlight curvature regimes where the parallel orientation is more favorable ($\Delta F < 0$). (e,f) Corresponding curves for the free energy per area (red) and thickness (green) in the perpendicular configuration C_\perp .

but also to generate defects at specific regions in space.

Fig. 4 also shows the behavior of the free energy and the minimum-energy thickness as a function of mean curvature for the C_\perp configuration. For $H \geq 0$, the free energy increases as the curvature increases, indicating that the thin film is likely to become unstable and dewet from the substrate, also in good agreement with the experimental data shown in Fig. 2. Conversely, for $H < 0$ the film remains stable, since the free energy decreases as the curvature increases. In the experiments (Fig. 2), it can be observed that the thin film dewets at the region with the highest curvature, where $H_{max} R_g \sim 0.015$. These results are in good agreement with recent experiments on curved substrates by Park and Tsarkova [49], who also found dewetting for $H > 0$ and thin film thickening for $H < 0$ in agreement with Fig. 4(e), 4(f) (green curves).

In conclusion, we have shown through experiments, symmetry considerations, and SCFT calculations that curvature can be employed as a guiding field to produce well-ordered patterns. The SCFT calculations provide a rough estimate of the equilibrium configuration for curved systems and predict dewetting in regions with high local positive curvature $H > 0$. From a technological perspective, our results indicate that through appropriate control over the surface interactions, it should be possible to prevent dewetting while keeping a geometric field with sufficient strength to guide order.

ACKNOWLEDGEMENTS

We gratefully acknowledge the financial support from the Deutsche Forschungsgemeinschaft (Grant Schm 985/19 and SFB TRR 146), the National Science Foundation MRSEC Program through the Princeton Center for Complex Materials (DMR-1420541), the Universidad Nacional del Sur, and the National Research Council of Argentina (CONICET). The SCFT calculations were done on the high performance computing center MOGON in Mainz. PS-PEP 4/13 was synthesized by Dr. Douglas Adamson.

* gianthvu@uni-mainz.de

† dvega@uns.edu.ar

‡ friederike.schmid@uni-mainz.de

- [1] C. Harrison, D. H. Adamson, Z. D. Cheng, J. M. Sebastian, S. Sethuraman, D. A. Huse, R. A. Register, and P. M. Chaikin, *Science* **290**, 1558 (2000).
- [2] R. A. Segalman, *Mater. Sci. Eng. R* **48**, 191 (2005).
- [3] I. Bitai, J. K. W. Yang, Y. S. Jung, C. A. Ross, E. L. Thomas, and K. K. Berggren, *Science* **321**, 939 (2008).
- [4] R. Ruiz, H. Kang, F. A. Detcheverry, E. Dobisz, D. S. Kercher, T. R. Albrecht, J. J. de Pablo, and P. F. Nealey, *Science* **321**, 936 (2008).
- [5] G. Singh, K. G. Yager, B. Berry, H.-C. Kim, and A. Karim, *ACS Nano* **6**, 10335 (2012).
- [6] A. P. Marencic and R. A. Register, *Annu. Rev. Chem. Biomol. Eng.* **1**, 277 (2010).
- [7] D. A. Vega, L. R. Gómez, A. D. Pezzutti, F. Pardo, P. M. Chaikin, and R. A. Register, *Soft Matter* **9**, 9385 (2013).
- [8] N. A. García, A. D. Pezzutti, R. A. Register, D. A. Vega, and L. R. Gómez, *Soft Matter* **11**, 898 (2015).
- [9] A. A. Abate, G. T. Vu, A. D. Pezzutti, N. A. García, R. L. Davis, F. Schmid, R. A. Register, and D. A. Vega, *Macromolecules* **49**, 7588 (2016).
- [10] C. Harrison, Z. Cheng, S. Sethuraman, D. A. Huse, P. M. Chaikin, D. A. Vega, J. M. Sebastian, R. A. Register, and D. H. Adamson, *Phys. Rev. E* **66**, 011706 (2002).
- [11] D. A. Vega, C. K. Harrison, D. E. Angelescu, M. L. Trawick, D. A. Huse, P. M. Chaikin, and R. A. Register, *Phys. Rev. E* **71**, 061803 (2005).
- [12] U. Nagpal, M. Müller, P. F. Nealey, and J. J. de Pablo, *ACS Macro Lett.* **1**, 418 (2012).
- [13] S.-M. Hur, V. Thapar, A. Ramírez-Hernández, G. Khaira, T. Segal-Peretz, P. A. Rincon-Delgadillo, W. Li, M. Müller, P. F. Nealey, and J. J. de Pablo, *Proc. Natl. Acad. Sci. USA* **112**, 14144 (2015).
- [14] D. E. Angelescu, J. H. Waller, D. H. Adamson, P. Deshpande, S. Y. Chou, R. A. Register, and P. M. Chaikin, *Adv. Mater.* **16**, 1736 (2004).
- [15] S. Y. Kim, A. Nunns, J. Gwyther, R. L. Davis, I. Manners, P. M. Chaikin, and R. A. Register, *Nano Lett.* **14**, 5698 (2014).
- [16] R. L. Davis, B. T. Michal, P. M. Chaikin, and R. A. Register, *Macromolecules* **48**, 5339 (2015).
- [17] K. Amundson, E. Helfand, X. Quan, and S. D. Smith, *Macromolecules* **26**, 2698 (1993).
- [18] T. L. Morkved, M. Lu, A. M. Urbas, E. E. Ehrichs, H. M. Jaeger, P. Mansky, and T. P. Russell, *Science* **273**, 931 (1996).
- [19] P. Mansky, J. DeRouchey, T. P. Russell, J. Mays, M. Pitsikalis, T. Morkved, and H. Jaeger, *Macromolecules* **31**, 4399 (1998).
- [20] B. C. Berry, A. W. Bosse, J. F. Douglas, R. L. Jones, and A. Karim, *Nano Lett.* **7**, 2789 (2007).
- [21] K. G. Yager, N. J. Fredin, X. Zhang, B. C. Berry, A. Karim, and R. L. Jones, *Soft Matter* **6**, 92 (2010).
- [22] S. O. Kim, H. H. Solak, M. P. Stoykovich, N. J. Ferrier, J. J. de Pablo, and P. F. Nealey, *Nature* **424**, 411 (2003).
- [23] L. R. Gómez and D. A. Vega, *Phys. Rev. E* **79**, 031701 (2009).
- [24] N. A. García, R. L. Davis, S. Y. Kim, P. M. Chaikin, R. A. Register, and D. A. Vega, *RSC Adv.* **4**, 38412 (2014).
- [25] M. Luo, D. M. Scott, and T. H. Epps III, *ACS Macro Letters* **4**, 516 (2015).
- [26] D. Sundrani, S. B. Darling, and S. J. Sibener, *Nano Lett.* **4**, 273 (2004).
- [27] I. W. Hamley, *Prog. Polym. Sci.* **34**, 1161 (2009).
- [28] D. R. Nelson, *Nano Lett.* **2**, 1125 (2002).
- [29] E. A. Matsumoto, D. A. Vega, A. D. Pezzutti, N. A. García, P. M. Chaikin, and R. A. Register, *Proc. Natl. Acad. Sci. USA* **112**, 12639 (2015).
- [30] A. D. Pezzutti, L. R. Gómez, and D. A. Vega, *Soft Matter* **11**, 2866 (2015).
- [31] M. Müller and F. Schmid, *Adv. Polym. Sci.* **185**, 1 (2005).
- [32] M. Deserno, *Handbook of Modern Biophysics: Membrane Elasticity and Mediated Interactions in Continuum Theory: A Differential Geometric Approach* (Publisher Humana Press, 2009).
- [33] A. P. Marencic, D. H. Adamson, P. M. Chaikin, and R. A. Register, *Phys. Rev. E* **81**, 011503 (2010).
- [34] C. D. Santangelo, V. Vitelli, R. D. Kamien, and D. R. Nelson, *Phys. Rev. Lett.* **99**, 017801 (2007).
- [35] R. D. Kamien, D. R. Nelson, C. D. Santangelo, and V. Vitelli, *Phys. Rev. E* **80**, 051703 (2009).
- [36] W. Helfrich, *Z. Naturforsch. C* **28**, 693 (1973).
- [37] P. B. Canham, *J. Theor. Biol.* **26**, 61 (1970).
- [38] T. Powers and P. Nelson, *J. Physique II* **5**, 1671 (1995).
- [39] P. Biscari and E. M. Terentjev, *Phys. Rev. E* **73**, 051706 (2006).
- [40] R. Oda, I. Huc, M. Schmutz, S. J. Candau, and F. C. MacKintosh, *Nature* **399**, 566 (1999).
- [41] C.-M. Chen, *Phys. Rev. E* **59**, 6192 (1999).
- [42] G. Napoli and L. Vergori, *Phys. Rev. Lett.* **108**, 207803 (2012).
- [43] G. Napoli and L. Vergori, *Phys. Rev. E* **85**, 061701 (2012).
- [44] M. W. Matsen, *J. Phys.: Cond. Matter* **14**, R21 (2002).
- [45] In Ref. [9], $\mu = (2.5 + \ln G)k_B T$ was used. Here we had to slightly increase μ , otherwise films on curved substrates with positive curvature were not stable or metastable.
- [46] E. Helfand, *J. Chem. Phys.* **62**, 999 (1975).
- [47] This value is slightly larger than that obtained directly from $\langle R_0^2/M \rangle$ for the experimental systems according to Ref. [50], $R_g \approx 5.8$ nm. Similar discrepancies were observed in other block copolymer systems, e.g., [51].
- [48] A. Knoll, L. Tsarkova, and G. Krausch, *Nano Lett.* **7**, 843 (2007).
- [49] S. Park and L. A. Tsarkova, *Macromolecules* **50**, 6840 (2017).

- [50] L. J. Fetters, D. J. Lohse, D. Richter, T. A. Witten, and A. Zirkel, *Macromolecules* **27**, 4639 (1994).
- [51] K. Mori, H. Tanaka, H. Hasegawa, and T. Hashimoto, *Polymer* **30**, 1389 (1989).
- [52] Q. Pike, F. A. Detcheverry, M. Müller, and J. J. de Pablo, *Journal of Chemical Physics* **131** (2009), 10.1063/1.3187936.
- [53] F. A. Detcheverry, G. Liu, P. F. Nealey, and J. J. de Pablo, *Macromolecules* **43**, 3446 (2010).

SUPPLEMENTARY INFORMATION ON: CURVATURE AS A GUIDING FIELD FOR PATTERNS IN THIN BLOCK COPOLYMER FILMS

This supplementary material provides additional information about the experimental systems and details on the theory and the SCFT calculations.

Experimental Systems

System Preparation

The polystyrene-block-poly(ethylene-alt-propylene) diblock (PS-PEP 4/13) copolymer was synthesized through sequential living anionic polymerization of styrene and isoprene followed by selective saturation of the isoprene block (see ref. [33] for details). Thin films of thickness ~ 30 nm are prepared by spin-coating from a 1 wt. % solution in toluene.

To obtain a free-standing membrane, we first spin coat a monolayer of BC cylinders onto a 50 nm thick flat layer of sucrose deposited onto a silicon wafer, then thermally anneal it at $T=363\text{K}$ until a prescribed orientational correlation length of $\xi_2 \sim 200$ nm is obtained [29], and finally cool it to room temperature. The sucrose layer is then used as a sacrificial layer to float the thin film off the substrate and onto the surface of water, and subsequently redeposit it as a free-standing membrane on a transmission electron microscopy (TEM) grid (grid spacing $25\text{ }\mu\text{m} > \xi_2 > d_{sm}$). As the film is lifted off at a temperature well below the glass transition temperature of the PS block, the system retains the symmetry, average inter-cylinder distance, and structure of defects established during annealing. The pattern order is mainly disrupted by $\pm\frac{1}{2}$ disclination multipoles.

To prepare the substrate, we employ a solvent-annealing technique on a photoresist array of trench patterns deposited onto a silicon nitride wafer. Details about the method of substrate preparation can be found elsewhere [7]. It yields Gaussian-like smooth substrates with a pitch of $2.2\text{ }\mu\text{m}$ and crests with maximum height of 80 nm. The largest mean curvature of the substrate is found at the crests, where $H = H_{max} \sim 2.5\text{ }\mu\text{m}^{-1}$.

The thin films are imaged using a Veeco Dimension 3000 atomic force microscope (AFM) in tapping mode. The spring constant of the tip (uncoated Si) is $\sim 40\text{ N/m}$ and its resonant frequency is 300 kHz.

Membrane topography

In order to determine the local curvatures, the metric tensor for the membrane was obtained at room temperature from the AFM height profiles. Through AFM we

parametrize the surface in the Monge gauge. In this representation, the coordinates of each point \mathbf{r} are expressed as $\mathbf{r} = (x, y, h(x, y))$, where x and y are planar coordinates and $h(x, y)$ the out-of-plane displacement. The metric tensor can then be calculated as $g_{ij} = \delta_{ij} + h_i h_j$ and the shape tensor as

$$\mathbf{S} = \frac{1}{(1 + h_x^2 + h_y^2)^{3/2}} \begin{pmatrix} (1 + h_y^2)h_{xx} - h_x h_y h_{xy} & (1 + h_x^2)h_{xy} - h_{xx} h_x h_y \\ (1 + h_y^2)h_{xy} - h_x h_y h_{yy} & (1 + h_x^2)h_{yy} - h_{xy} h_x h_y \end{pmatrix}. \quad (\text{S1})$$

The Eigenvalues of \mathbf{S} give the principal curvatures. Standard methods are employed to determine the metric tensor and the principal curvatures at each point on the membrane surface [29].

Figure S1 shows the direction of the principal minimum and maximum curvatures. Once these directions and the principal radii of curvature $R_{1,2}$ have been determined, the geometric properties of the membrane shape can be obtained. To determine the correlation between the pattern orientation α and membrane distortions, we determine the local orientation of the membrane wrinkles β relative to the x-axis from the distribution of the maximum main curvature k_1 . The wrinkle orientation β was obtained by measuring the local gradient of k_1 (see Fig. S2), i.e. $\tan(\beta) = \nabla_y K_1 / \nabla_x K_1$.

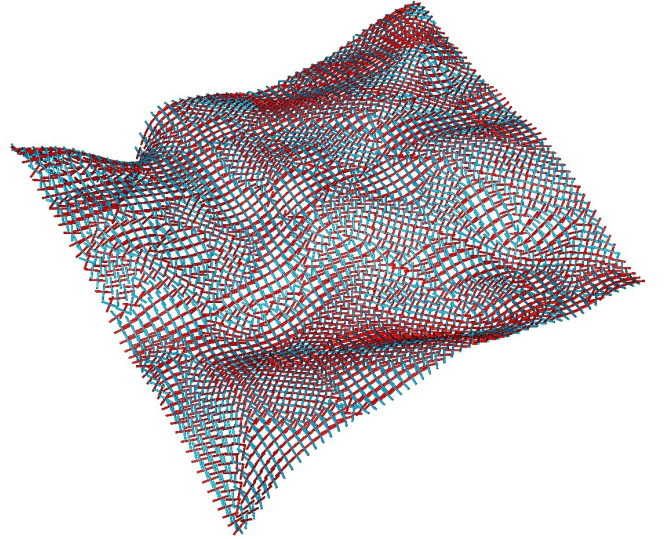


FIG. S1. Unit vectors indicating the directions of the principal maximum (red lines) and minimum (light blue lines) curvatures.

Figs. S3 and S4 show the mean and Gaussian curvatures for a free-standing cylinder-forming BC thin film membrane. Here a semitransparent mask with the maps for H and K was applied to also show the block copolymer texture (70% transparency).

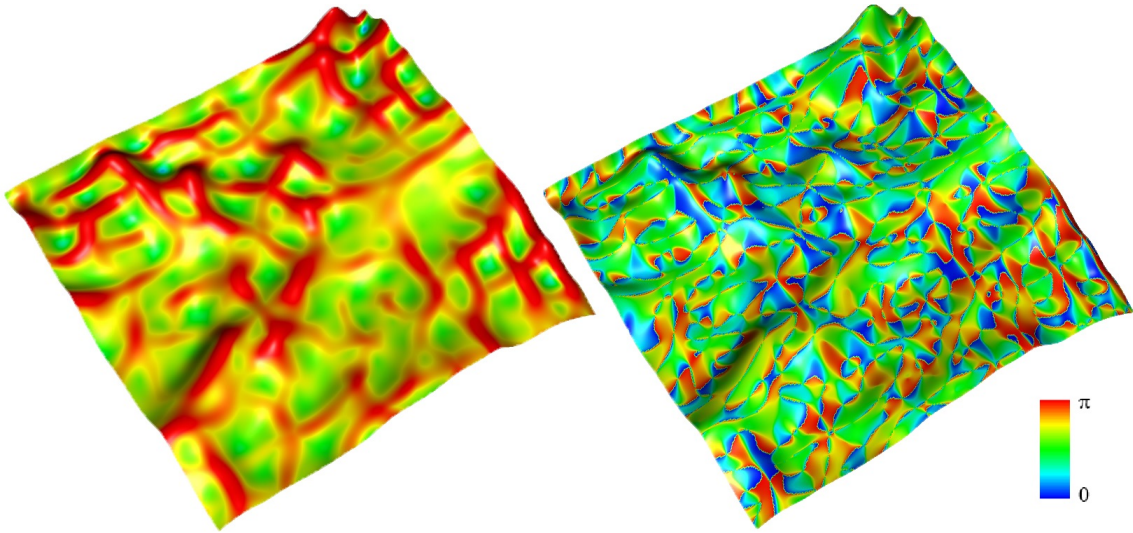


FIG. S2. Local values of maximum principal curvature allow clear identification of the location and local orientation β of the membrane wrinkles. Left panel: maximum principal curvature. Right panel: orientation β of the wrinkles with regard to the x-axis.

Note the wrinkled topography of the membrane and the coupling with the smectic-like texture of the BC system.

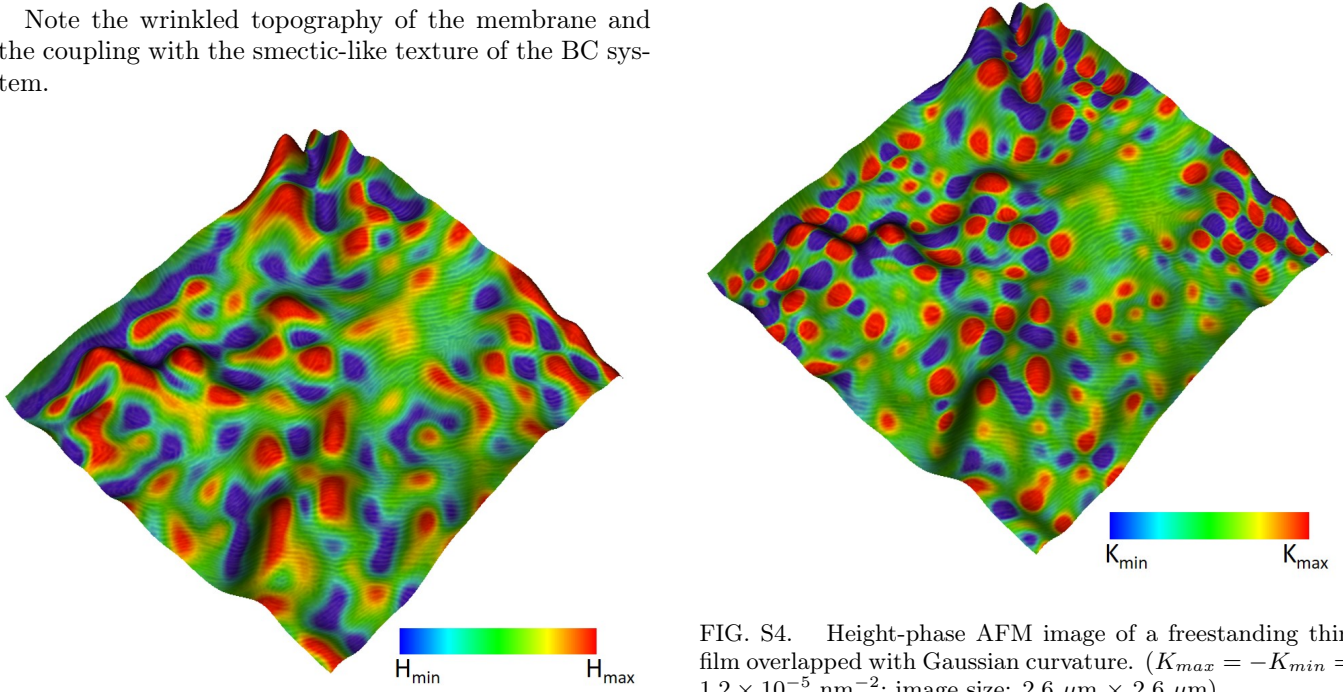


FIG. S3. Height-phase AFM image of a freestanding thin film overlapped with mean curvature. ($H_{max} = -H_{min} = 3.84 \times 10^{-3} \text{ nm}^{-1}$; image size: $2.6 \mu\text{m} \times 2.6 \mu\text{m}$).

FIG. S4. Height-phase AFM image of a freestanding thin film overlapped with Gaussian curvature. ($K_{max} = -K_{min} = 1.2 \times 10^{-5} \text{ nm}^{-2}$; image size: $2.6 \mu\text{m} \times 2.6 \mu\text{m}$).

Thin films on curved substrates

Fig. S5 emphasizes the coupling between the pattern orientation and the mean curvature of the substrate. As here the Gaussian curvature is zero, the substrate is

topologically equivalent to flat space. Thus, while for a strictly 2D system no coupling can be expected, the finite thickness of the film leads to an interaction that penalizes those configurations that involve an inter-cylinder elastic distortion.

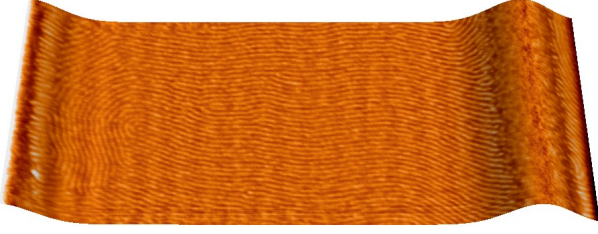


FIG. S5. (a) 3D AFM phase-height image of the BC thin film lying on a curved substrate after 3.5 h of thermal annealing at $T=373\text{K}$. (image size: $2.5\text{ }\mu\text{m} \times 1.0\text{ }\mu\text{m}$).

Theory: Symmetry considerations.

In its own Eigensystem, the shape tensor \mathbf{S} can be written as $\mathbf{S} = \sum_{i=1}^2 k_i \mathbf{u}_i \otimes \mathbf{u}_i$, where k_i are the principal curvatures and \mathbf{u}_i the corresponding Eigenvectors, where we can choose $|k_1| > |k_2|$ without loss of generality. If a membrane or thin film has in-plane order characterized by a director field \mathbf{n} , the curvature free energy per area no longer has to be rotationally symmetric, and it may contain additional terms of the form $(\mathbf{n} \cdot \mathbf{S} \cdot \mathbf{n})$, $(\mathbf{n} \cdot \mathbf{S} \cdot \mathbf{n})^2$, and $(\mathbf{n} \cdot \mathbf{S})^2$. We write the contribution of these terms to the curvature free energy per area in the general form

$$F_{\mathbf{n}} = A\mathbf{n} \cdot \mathbf{S} \cdot \mathbf{n} - B(\mathbf{n} \cdot \mathbf{S} \cdot \mathbf{n})^2 - C(\mathbf{n} \cdot \mathbf{S})^2. \quad (\text{S2})$$

The product $(\mathbf{n} \cdot \mathbf{u}_1)$ defines the angle θ between the director and the direction of largest curvature *via* $(\mathbf{n} \cdot \mathbf{u}_1)^2 = \cos^2 \theta$. Inserting this and using $\mathbf{n} = (\mathbf{n} \cdot \mathbf{u}_1)\mathbf{u}_1 + (\mathbf{n} \cdot \mathbf{u}_2)\mathbf{u}_2$ and $(\mathbf{n} \cdot \mathbf{u}_2)^2 = 1 - (\mathbf{n} \cdot \mathbf{u}_1)^2$, we obtain

$$\begin{aligned} F_{\mathbf{n}} = & AH - \left(\frac{3}{2}B + 2C\right)H^2 + \left(\frac{1}{2}B + C\right)K \\ & + \left(\frac{A}{2}(k_1 - k_2) - (B + C)(k_1 - k_2)H\right) \cos(2\theta) \\ & - \frac{B}{2}(H^2 - K) \cos(4\theta). \end{aligned} \quad (\text{S3})$$

The first term can be absorbed in the spontaneous curvature c_0 , and the second two terms in the bending and Gaussian modulus κ_b and κ_g , respectively. The last two terms give the expression for the anisotropic curvature free energy per area F_{ani} in the main text (Eq. (1)), with $\kappa' = (B + C)$ and $\kappa'' = B$, and $c'_0 = A/(B + C)$.

Theory: SCFT calculations.

Basic equations

We consider a melt of asymmetric AB diblock copolymer molecules confined in a volume V between two coaxial cylindrical surfaces of radius R_1 and $R_2 = R_1 + \epsilon$, where ϵ is the thickness of the confined film. The two surfaces preferentially attract A -monomers. Dirichlet boundary conditions are applied in the radial direction

and periodic boundary conditions are applied in the in-plane directions. Each diblock copolymer molecule consists of N segments of which a fraction f forms the majority block A . We assume that A and B segments have the same statistical segment length b . The microscopic concentration operators of A and B segments at a given point $\mathbf{r}(r, \varphi, z)$ are defined as

$$\hat{\phi}_A(\mathbf{r}) = \frac{1}{\rho_c} \sum_{j=1}^n \int_0^f ds \delta(\mathbf{r} - \mathbf{r}_j(s)) \quad (\text{S4})$$

$$\hat{\phi}_B(\mathbf{r}) = \frac{1}{\rho_c} \sum_{j=1}^n \int_f^1 ds \delta(\mathbf{r} - \mathbf{r}_j(s)) \quad (\text{S5})$$

respectively. These concentrations are made dimensionless by dividing by the average copolymer density ρ_c . The interaction potential of the melt is

$$\begin{aligned} \frac{\mathcal{H}_{\mathcal{I}}}{k_B T} = & \rho_c \int d\mathbf{r} \left[\chi N \hat{\phi}_A(\mathbf{r}) \hat{\phi}_B(\mathbf{r}) \right. \\ & + \frac{1}{2} \kappa N \left(\hat{\phi}_A(\mathbf{r}) + \hat{\phi}_B(\mathbf{r}) - 1 \right)^2 \Big] \\ & + \rho_c \int d\mathbf{r} H(\mathbf{r}) \left[\Lambda_{A,B}^{s,a} N \hat{\phi}_A(\mathbf{r}) + \Lambda_B^{s,a} N \hat{\phi}_B(\mathbf{r}) \right] \end{aligned} \quad (\text{S6})$$

where the Flory-Huggins parameter χ specifies the repulsion of A and B segments. The second term describes a finite compressibility of the melt [46], which is fixed to $\kappa N = 25$, similar to previous work on similar systems [52, 53]. The terms $\Lambda_{A,B}^{s,a} H(\mathbf{r})$ are surface fields. We choose a form

$$H(\mathbf{r}) = \begin{cases} (1 + \cos(\pi(r - R_1)/\delta)) & R_1 \leq r \leq R_1 + \delta \\ 0 & R_1 + \delta < r < R_2 - \delta \\ (1 + \cos(\pi(R_2 - r)/\delta)) & R_2 - \delta \leq r \leq R_2 \end{cases} \quad (\text{S7})$$

with $\delta = 0.2R_g$. The value of δ must be chosen small enough relative to the domain size so that its finite size does not affect the phase behavior of the thin films significantly. $\Lambda_{A,B}^{s,a}$ gives the strength of the interaction between block A or B , respectively, and the substrate (s) and air (a) interface. The “surface interaction energies per area” of component A or B are defined as the integrated surface energy per area of a hypothetical film of A or B monomers with density $\hat{\phi}_{A,B} \equiv 1$, i.e., $\gamma_{A,B}^{s,a} = \rho_c \int d\mathbf{r} H(\mathbf{r}) \Lambda_{A,B}^{s,a}$. They will be given in units of $\hat{\gamma} = \rho_c R_g k_B T$ (which is a unit of energy per area). In the following, we shall set $k_B T = 1$, for notational simplicity.

In the membrane study we assume that the two surfaces are symmetric for each block, $\Lambda_A^a N = -120$ and $\Lambda_B^a N = -115$ corresponding to $\gamma_A N = -24\hat{\gamma}$ and $\gamma_B N = -23\hat{\gamma}$. In the curved supported thin films, we choose symmetric surface interactions for the B -block $\Lambda_B^s N = \Lambda_B^a N = -30$ corresponding to $\gamma_B N = -6\hat{\gamma}$, and asymmetric conditions for the A -block. Specifically, we study two cases:

- I. The substrate attracts the A -block more strongly than the free (air) surface ($\Lambda_A^s N = -120, \Lambda_A^a N = -50$) with corresponding surface energy per area $\gamma_A^s N = -24\hat{\gamma}, \gamma_A^a N = -10\hat{\gamma}$.
- II. The free surface attracts the A -block more strongly than the substrate ($\Lambda_A^s = -50, \Lambda_A^a N = -100$) with corresponding surface energy per area $\gamma_A^s N = -10\hat{\gamma}$ and $\gamma_A^a N = -20\hat{\gamma}$.

Our calculations are done in the grand canonical ensemble with the free energy

$$\begin{aligned}
F_{GC} = & -e^\mu Q + \rho_c \int d\mathbf{r} [\chi N \phi_A(\mathbf{r}) \phi_B(\mathbf{r}) \\
& + \frac{\kappa}{2} (\phi_A(\mathbf{r}) + \phi_B(\mathbf{r}) - 1)^2] \\
& - \rho_c \int d\mathbf{r} [\omega_A(\mathbf{r}) \phi_A(\mathbf{r}) + \omega_B(\mathbf{r}) \phi_B(\mathbf{r})] \\
& + \rho_c \int d\mathbf{r} H(\mathbf{r}) N [\Lambda_A^{s,a} \phi_A(\mathbf{r}) + \Lambda_B^{s,a} \phi_B(\mathbf{r})] \quad (\text{S8})
\end{aligned}$$

where μ is chemical potential, Q the partition function of a single non-interacting polymer chain,

$$Q = \int d\mathbf{r} q(\mathbf{r}, s) q^\dagger(\mathbf{r}, 1-s) \quad (\text{S9})$$

and $q(\mathbf{r}, s)$ and $q^\dagger(\mathbf{r}, 1-s)$ satisfy the modified diffusion equation

$$\frac{\partial q(\mathbf{r}, s)}{\partial s} = \Delta q(\mathbf{r}, s) - \omega_\alpha(\mathbf{r}, s) q(\mathbf{r}, s) \quad (\text{S10})$$

with

$$\omega_\alpha(\mathbf{r}, s) = \begin{cases} \omega_A(\mathbf{r}) & \text{for } 0 < s < f \\ \omega_B(\mathbf{r}) & \text{for } f < s < 1 \end{cases} \quad (\text{S11})$$

and the initial condition $q(\mathbf{r}, 0) = 1$. The diffusion equation for $q^\dagger(\mathbf{r}, 1-s)$ is similar with $\omega_\alpha(\mathbf{r}, s)$ replaced by $\omega_\alpha(\mathbf{r}, 1-s)$ and the same initial condition, $q^\dagger(\mathbf{r}, 0) = 1$. By finding the extremum of the free energy, Eq. (S8) with respect to $\omega_{A,B}(\mathbf{r})$ and $\phi_{A,B}(\mathbf{r})$, we get the self-consistent equations,

$$\begin{aligned}
\frac{\omega_A(\mathbf{r})}{N} &= \chi \phi_B(\mathbf{r}) + \kappa [\phi_A(\mathbf{r}) + \phi_B(\mathbf{r}) - 1] + \Lambda_A H(\mathbf{r}) \\
\frac{\omega_B(\mathbf{r})}{N} &= \chi \phi_A(\mathbf{r}) + \kappa [\phi_A(\mathbf{r}) + \phi_B(\mathbf{r}) - 1] + \Lambda_B H(\mathbf{r}) \\
\phi_A(\mathbf{r}) &= \frac{1}{\rho_c} e^\mu \int_0^f ds q(\mathbf{r}, s) q^\dagger(\mathbf{r}, 1-s) \\
\phi_B(\mathbf{r}) &= \frac{1}{\rho_c} e^\mu \int_f^1 ds q(\mathbf{r}, s) q^\dagger(\mathbf{r}, 1-s) \quad (\text{S12})
\end{aligned}$$

Boundary conditions

The SCFT calculations are done in cylindrical coordinates (r, ϕ, z) , where r is the direction normal to the

film or membrane surface and z is the direction of zero curvature. Configurations C_\parallel, C_\perp with cylinder orientations parallel or perpendicular to the direction of curvature can be obtained with periodic boundary conditions in the (ϕ, z) directions. In order to impose a given tilted orientation with tilt angle θ (as in Fig. 3c, inset), we must apply tilted boundary conditions, either in the z or in the ϕ direction. We do this by using affine coordinates (r, u, v) with periodic boundary conditions in (u, v) and (1) $u = \varphi, v = z - \varphi a, a = R \tan \theta$ or (2) $(r, u, v), u = \varphi - bz, v = z, b = 1/(R \tan \theta)$. In case (1), $a = 0$ corresponds to the perpendicular configuration C_\perp ($\theta = 0$), and in case (2) $b = 0$ corresponds to the parallel configuration C_\parallel ($\theta = \pi/2$).

We solve the modified diffusion equations with periodic boundary conditions in effectively two dimensions: (r, v) , independent of u in case (1), and (r, u) , independent of v in case (2). This enforces tilted orientations of cylinders. In general, the Laplace-Beltrami operator has the following form

$$\Delta_{LB} = \frac{1}{\sqrt{|\det g|}} \sum_{ij} \frac{\partial}{\partial x_i} \left(g^{ij} \sqrt{|\det g|} \frac{\partial}{\partial x_j} \right) \quad (\text{S13})$$

where g_{ij} is the metric tensor and g^{ij} its inverse. The Laplace-Beltrami operator in cases (1) and (2) is thus given by

$$\begin{aligned}
\Delta_{LB}^{(1)} = & \frac{1}{r} \frac{\partial}{\partial r} + \frac{\partial^2}{\partial r^2} + \frac{1}{r^2} \frac{\partial^2}{\partial u^2} - \frac{2a}{r^2} \frac{\partial^2}{\partial u \partial v} \\
& + \left(1 + \frac{a^2}{r^2} \right) \frac{\partial^2}{\partial v^2} \quad \text{case (1)} \quad (\text{S14})
\end{aligned}$$

$$\begin{aligned}
\Delta_{LB}^{(2)} = & \frac{1}{r} \frac{\partial}{\partial r} + \frac{\partial^2}{\partial r^2} + \left(\frac{1}{r^2} + b^2 \right) \frac{\partial^2}{\partial u^2} \\
& - 2b \frac{\partial^2}{\partial u \partial v} + \frac{\partial^2}{\partial v^2} \quad \text{case (2)}. \quad (\text{S15})
\end{aligned}$$

The modified diffusion equations were solved using the Crank-Nicolson method. We used the setup (1) for small angles $0 < \theta < \pi/4$ and the setup (2) for large angles $\pi/4 < \theta < \pi/2$, and compared the results from both setups at the angle $\theta = \pi/4$, to verify that both setups give the same result.

Discretization errors and correction

The discretizations in the azimuthal and thin film directions (z and r , respectively) were chosen as $\Delta z = 0.05 R_g$ and $\Delta r = 0.01 R_g$, and the parameter s was discretized in steps of $\Delta s = 0.0001$. Whereas most of the choices are not critical, we found that the discretization in the r direction has a significant influence on the resulting free energies, and discretization errors could not be neglected. On the other hand, we also found that they lead to an energy shift ΔF which depends only on Δr

and not on the film thickness or curvature. We therefore studied the dependence of ΔF on Δr systematically for different values of the film thickness and curvature. Then we fitted the result to a third order polynomial, resulting in the estimate $\Delta F(\Delta r) = -11.75\Delta r - 270\Delta r^2 + 5035\Delta r^3$ ($\Delta F(\Delta r) = -11.95\Delta r - 167\Delta r^2 + 3737\Delta r^3$) and $\Delta F(\Delta r) = -12.6\Delta r - 277\Delta r^2 - 2367\Delta r^3$ with asymmetric and homogeneous surface interactions, respectively. Figs. S6, S7 and S8 present the fitting results. These corrections were then applied to the results of the SCFT calculations.

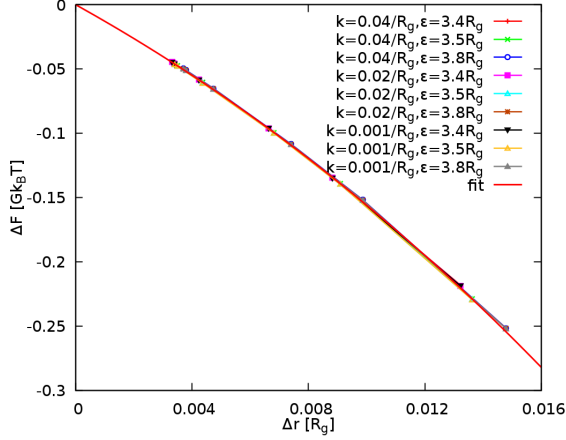


FIG. S6. Shift of free energy ΔF as a function of discretization Δr for symmetric films with surface interactions $\Lambda_A^s N = -120, \Lambda_B^s N = -115$, for different curvatures and film thicknesses ϵ as indicated. Solid line: fit function $f(x) = -12.6x - 277x^2 - 2367x^3$.

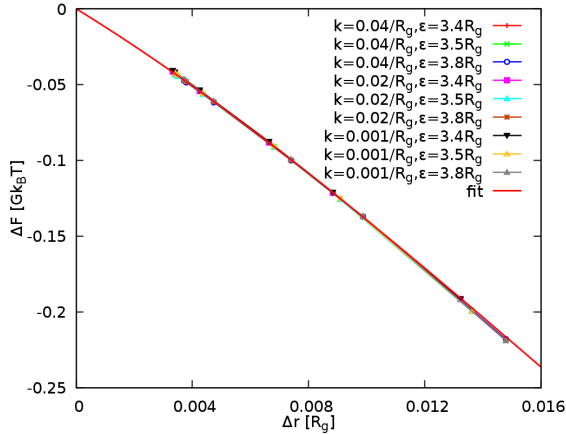


FIG. S7. Shift of free energy ΔF as a function of discretization Δr for films with asymmetric surface interactions $\Lambda_A^s N = -120, \Lambda_B^s N = -30$ at the fixed substrate and $\Lambda_A^a N = -50, \Lambda_B^a N = -30$ at the free surface for different curvatures and film thicknesses ϵ as indicated. Solid line: fit function $f(x) = -11.75x - 270x^2 + 5035x^3$.

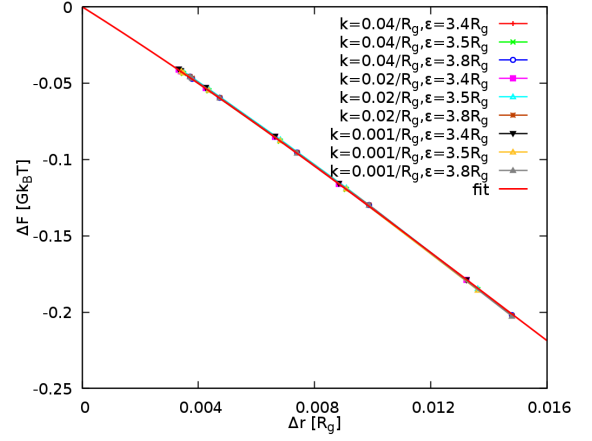


FIG. S8. Shift of free energy ΔF as a function of discretization Δr for films with asymmetric surface interactions $\Lambda_A^s N = -50, \Lambda_B^s N = -30$ at the fixed substrate and $\Lambda_A^a N = -100, \Lambda_B^a N = -30$ at the free surface for different curvatures and film thicknesses ϵ as indicated. Solid line: fit function $f(x) = -11.95x - 167x^2 + 3737x^3$.

Optimum thickness of free-standing membranes

Fig. S9 shows the behavior of the optimum film thickness of free-standing membranes as a function of curvature both parallel and perpendicular configurations. Interestingly, the optimal thickness is not affected strongly by curvature in the range of curvatures considered here.

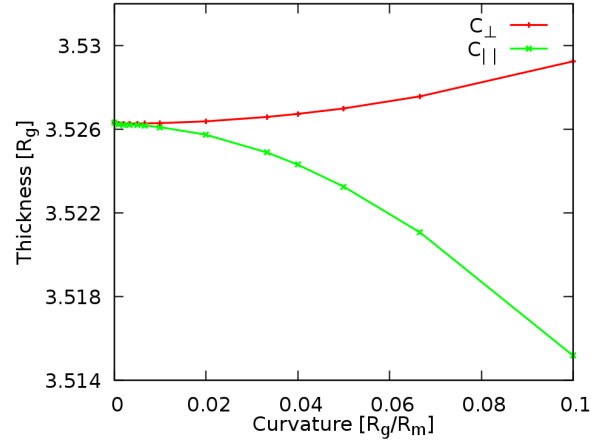


FIG. S9. The optimal film thickness of free-standing membranes as a function of curvature.